Applied Catalysis B: Environmental 130–131 (2013) 132–142

Contents lists available at SciVerse ScienceDirect

Applied Catalysis B: Environmental

journal homepage: www.elsevier.com/locate/apcatb

Preparation and application of thermosensitive poly(NIPAM-*co*-MAH-β-CD)/(TiO_2-MWCNTs) composites for photocatalytic degradation of dinitro butyl phenol (DNBP) under visible light irradiation

Hui-Long Wang[a], Yan Li[a], Li Pang[a], Wen-Zhu Zhang[b], Wen-Feng Jiang[a,*]

[a] Department of Chemistry, Dalian University of Technology, Dalian 116023, China
[b] Experimental Center of Chemistry, Dalian University of Technology, Dalian 116023, China

ARTICLE INFO

Article history:
Received 28 June 2012
Received in revised form
22 September 2012
Accepted 29 September 2012
Available online 8 November 2012

Keywords:
Titania
Thermosensitive composite
Photocatalyst
Photocatalytic degradation
Alkyl dinitro phenol

ABSTRACT

Based on the unique temperature responsive characters of polymeric material based on *N*-isopropylacrylamide (NIPAM), a capacity for organic molecular inclusion of maleic anhydride (MAH) modified β-cyclodextrin (β-CD), and the enhancements in photocatalytic activity of TiO_2 doped with multi-walled carbon nanotubes (MWCNTs), the novel thermosensitive poly(NIPAM-*co*-MAH-β-CD)/(TiO_2-MWCNTs) composite photocatalysts were prepared by UV light photoinitiating method. Fourier transform infrared spectra (FTIR), X-ray diffraction (XRD), thermal gravimetric analysis (TGA), X-ray photoelectron spectroscopy (XPS), transmission electron microscopy (TEM), BET surface area and UV–Vis diffuse reflectance spectra (UV–Vis/DRS) were used to characterize the structure, morphology and composition of the as-prepared composites. Results showed that TiO_2-MWCNTs nanoparticles were embedded evenly within the thermally responsive copolymer of NIPAM and MAH-β-CD. The thermoresponsive property of the synthesized composites was investigated by using swelling ratio measurements. The photocatalytic performances of the thermosensitive composite catalysts were evaluated for the degradation of 2-*sec*-butyl-4,6-dinitrophenol (DNBP) solution under visible light irradiation. The effect of operational parameters, i.e. pH of the solution, catalyst concentration, irradiation time, initial DNBP concentration on the photocatalytic degradation efficiency was explored and the results obtained were fitted with modified Langmuir–Hinshelwood model to investigate the degradation kinetics and discussed in detail. The repeatability of photocatalytic activity was also tested. The thermosensitive composite photocatalysts exhibited easy separation and less deactivation after several runs. A plausible mechanism is proposed for the photocatalytic degradation pathway of DNBP. The results of this study showed the feasible and potential use of the thermosensitive composites in photodegradation of organic pollutants by controlling temperature simply.

1. Introduction

Alkyl dinitro phenols constitute an important family of toxic refractory chemicals, which can be detrimental to human health and the environment. 2-*Sec*-butyl-4,6-dinitrophenol (DNBP) is a typical example of this class of toxic compounds. DNBP is extensively used in petrochemical industry as polymerization inhibitor for vinyl aromatics and in agriculture as herbicide [1,2]. Widespread use of this compound has led to contamination of soils, waste streams and surface waters. DNBP is a highly toxic compound classified as environmental chemical carcinogen and the maximum contaminant level (MCL) accepted for DNBP in drinking water is 7 ng mL^{-1} according to EPA [3]. DNBP is very chemically stable and this trait leads to removal of this compound from water was not accomplished completely by conventional wastewater treatment technologies. Also, due to difficult conditions for surviving microorganisms, biological processes encountered various limitations. Thus, finding the new treatment methods which would conduct complete decomposition of DNBP is highly desired.

In this context, advanced oxidation processes (AOPs) based on catalytic or chemical photooxidation have been proposed as alternative routes for water purification. AOPs act based on the formation of powerful and unstable species with high reactivity tendency (e.g. $^{\bullet}OH$, $O_2^{\bullet-}$, H_2O_2) to mineralize the resistant organic materials to harmless materials such as CO_2 and H_2O [4,5]. Among them, heterogeneous photocatalysis utilizing titanium dioxide (TiO_2) seems to be the most attractive method for water decontamination [6]. The reason for the increased interest in this method is that the process can be carried out under ambient conditions and TiO_2 has the advantages of high chemical stability,

* Corresponding author. Tel.: +86 411 84706295; fax: +86 411 84708590.
E-mail address: dlutjiangwf@yahoo.com.cn (W.-F. Jiang).

0926-3373/$ – see front matter © 2012 Elsevier B.V. All rights reserved.
http://dx.doi.org/10.1016/j.apcatb.2012.09.059

high photocatalytic activity, nontoxicity and relative low price [7]. However, uses of TiO_2 nanoparticles in applications such as wastewater treatment have been limited because there are major bottleneck drawbacks associated with TiO_2 photocatalysts, namely, low photo-quantum efficiency arising from the fast recombination of photo-generated electrons and holes, low efficiency for utilizing solar light due to its large band gap ($E_{g,\ anatase}$ = 3.2 eV), low capacity for the adsorption of organic pollutants and the problem of separation and recovery of nanometer sized TiO_2 particles from water.

Many techniques have been examined to not only extend the spectral response of TiO_2 into the visible region but also reduce the recombination of photo-generated electrons and photo-generated holes, thus enhancing its photocatalytic activity. Recently, some studies have reported that doping with suitable non-metal atoms is a useful way for improving the above two performances of TiO_2. There have been some papers published about improved TiO_2 photocatalysts doped with carbon [8,9], nitrogen [10,11], sulfur [12] or using codoped materials [13,14]. We have demonstrated that multi-walled carbon nanotubes (MWCNTs) can sensitize TiO_2 efficiently and the TiO_2-MWCNTs composite photocatalysts can be activated by absorbing both ultraviolet and visible light [15,16]. Since the photocatalytic reactions predominantly occur on the surface, the affinity interaction between TiO_2 and pollutants is the key factor that can influence the photocatalytic efficiency. The most commonly used method of enhancing the surface coverage of organic pollutants on catalyst is surface modification for TiO_2 particles [17–19]. Among the various surface modifiers, β-cyclodextrin (β-CD) is considered to be important owing to its special features such as torus structure, hydrophilic exterior, suitably sized hydrophobic cavity, easily tunable chemical properties and eco-friendly nature [20]. β-CD modified TiO_2 particles could adsorb and concentrate the organic pollutants from its aqueous solution and transfer it to the photocatalyst surface. The interaction between pollutants and the surface of β-CD modified TiO_2 was also enhanced to further promote the degradation of the pollutants. In addition, surface modification of nanocrystalline TiO_2 particles with β-CD may result in altered optical properties of nanoparticles compared to unmodified nanocrystallites [21]. Strategies that have been investigated to address the obstacle of separation and recovery of suspended fine TiO_2 catalyst particles from water include the synthesis of polymer–TiO_2 microcomposites. In recent years, the thermally responsive polymeric material based on *N*-isopropylacrylamide (NIPAM) has been extensively studied. Poly(*N*-isopropylacrylamide) (PNIPAM) displays a reversible and continuous phase transition behavior in response to a temperature change around 32 °C, which is termed as lower critical solution temperature (LCST) [22,23]. There are large variety of applications of PNIPAM, such as separation, drug-release control, enzyme fixation and phase-transfer catalysis [24–29]. The good environmental stability and temperature sensitive property make PNIPAM an ideal material for such applications. PNIPAM is a non-ionic polymer and usually prepared by free radical polymerization in aqueous solution using peroxide as initiator. Considering the unique temperature responsive characters of PNIPAM, it is expected that the combination of thermally responsive polymeric materials based on NIPAM with TiO_2 nanoparticles may enhance the dispersibility and reproducibility of TiO_2 particles [24,30]. Gupta et al. also reported that temperature sensitive polymer–TiO_2 microcomposites show rapid sedimentation with settling velocities nearly 100 times faster than pure TiO_2 and this would favor the separation and recovery of TiO_2 nanoparticles from pollutant degradation system [31].

Based on the unique temperature responsive characters of PNIPAM, a capacity for organic molecular inclusion of β-CD, and the enhancements in photocatalytic activity of TiO_2 doped with MWCNTs, in this work, the novel composites of poly (*N*-isopropylacrylamide-*co*-maleic anhydride-β-cyclodextrin)/(TiO_2-MWCNTs) (poly(NIPAM-*co*-MAH-β-CD)/(TiO_2-MWCNTs)) were prepared by UV light photoinitiating method. In this synthesis method, UV irradiation of the MWCNTs sensitized nanocrystalline TiO_2 generates active radicals to initiate polymerization reaction. Compared with the traditional heat-induced polymerization process [32], the UV light photoinitiating method has the following advantages: (i) TiO_2-MWCNTs nanoparticles play a role as reactant and initiator for free radical polymerization simultaneously and it is not necessary to add any additional chemical reagent in the synthesis of composites, (ii) the polymerization reaction rate can be controlled easily by controlling the UV light source, and (iii) the loss of TiO_2 particles during the polymerization process can be considerable reduced. The UV light photoinitiating synthesis technique resulted in composites with TiO_2-MWCNTS nanoparticles dispersing more uniformly within the thermoresponsive copolymer network. So, poly(NIPAM-*co*-MAH-β-CD)/(TiO_2-MWCNTs) composite catalysts can display better stability and higher photocatalytic activity when prepared via UV irradiation than via heat-induced polymerization reaction. Thermoresponsive and photocatalytic properties of the composite catalysts were integrated and expected to carry out "on–off" degradation by controlling the reaction temperature simply. The results reported here are critical and necessary inputs in the development of photocatalytic degradation/purification process that can use the novel polymer–TiO_2 composites from an academic as well as industrial point of view.

2. Experimental

2.1. Materials

TiO_2-MWCNTs nanoparticles (average particle size of 22 nm, specific surface area of 160 $m^2\ g^{-1}$) were prepared via sol–gel method in our laboratory. The details of the preparation procedures were similar to that described in our previous work [15,16]. *N*-isopropylacrylamide (NIPAM, 98%) was purchased from Tokyo Chemical Industry Co. Ltd. and recrystallized in hexane/acetone before use. β-cyclodextrin (β-CD) and maleic anhydride (MAH) were purchased from Tianjin Bodi Chemical Industrial Co. Ltd., China. 2-*Sec*-butyl-4,6-dinitrophenol (DNBP) was used as an alkyl dinitro phenol pollutant and obtained from Retell Fine Chemical Co. Ltd. (Tianjin, China). All other reagents used in this study were of AR grade from Tianjin Kermel Chemical reagent Co. Ltd., China and used without further purification. Double distilled water was used for preparation of the composite photocatalysts. A stock solution of DNBP (2.2×10^{-4} M) was prepared by dissolving DNBP in deionized water. Further solutions of different concentrations were made using the same stock solution.

2.2. Synthesis of poly(NIPAM-co-MAH-β-CD)/(TiO_2-MWCNTs) composites

β-CD (5.68 g, 5 mmol) and 4.90 g (50 mmol) of MAH were stirred in 30 mL of dimethylformamide for 10 h at 80 °C under a nitrogen atmosphere. After cooling to room temperature, 70 mL of acetone was added to the reaction solution. Afterwards, the reaction solution was filtered and the filtrate was collected. The filtrate was thoroughly washed with acetone and dried in vacuo at room temperature for 24 h. 7.02 g of reactive monomer, MAH modified β-CD (MAH-β-CD), was obtained.

The poly(NIPAM-*co*-MAH-β-CD)/(TiO_2-MWCNTs) composite photocatalysts were facilely prepared by the copolymerization of MAH-β-CD with NIPAM on the surface of TiO_2-MWCNTs in an aqueous solution using ultraviolet light photoinitiating method. A

typical procedure was as follows: 0.10 g TiO_2-MWCNTs nanoparticles were dispersed into 12 mL of double-distilled water. After sonication for 60 min, 0.68 g NIPAM and 0.29 g MAH-β-CD were added into the solution and stirred for 20 min to obtain a uniform suspension. Then the suspension was exposed to illumination of high-pressure mercury lamp (300 W) for 3 h to initiate the polymerization reaction. Afterward, the high-pressure mercury lamp was turned off and the polymerization reaction was allowed to proceed for 12 h at room temperature under gentle magnetic stirring without UV irradiation. The whole process was undertaken in a nitrogen atmosphere. After heating to 50 °C, the reaction mixture was then filtered, and the obtained composite was immersed in double-distilled water at room temperature for 6 days to remove some unreacted monomers, and the water was changed every several hours. Finally, the resulting product was dried to a constant weight in vacuo at 80 °C.

2.3. Characterization

Fourier transform infrared spectra (FTIR) of the samples were recorded on a Nicolet Avatar 360 spectrophotometer using conventional KBr pellets. The powder X-ray diffraction (XRD) patterns were taken for the samples using a computer controlled Rigaku D/MAX-2400 diffractometer with Cu Kα radiation (λ = 1.54184 Å) operating at 30 mA and 40 kV. The diffraction data were collected by using a continuous scan mode with a speed of 4.8° 2θ min^{-1}. The thermal gravimetric analysis (TGA) was performed by a Mettler-Toledo TGA/SDTA 851e analyzer (Switzerland) using an α-Al_2O_3 reference from room temperature to 850 °C in air atmosphere with a flow rate of 50 mL min^{-1} and a heating rate of 10 °C min^{-1}. X-ray photoelectron spectroscopy (XPS, VG ESCALAB 210) was used to determine surface composition of the synthesized thermally responsive composite samples. The morphology and particle size of the as-prepared composites were observed on a transmission electron microscope (TEM, FEI TECNAI G220 S-TWIN, America). The BET specific surface area of the catalyst was obtained on a JW-BK112 specific surface area and pore size analyzer (Beijing JWGB Sci & Tech Co. Ltd.). The UV–Vis diffuse reflectance spectra (UV–Vis/DRS) of the photocatalyst powder in the range 200–800 nm were recorded on a JASCO UV-550 ultraviolet spectrometer equipped with an integrating sphere using $BaSO_4$ as a reference.

2.4. Determination of pH_{pzc}

The pH of the point of zero charge (pH_{pzc}) was measured by pH drift method [33]. 50 mL of 0.05 mol L^{-1} NaCl solutions were placed in a series of conical borosilicate flasks, thermostatted at 25 °C, and N_2 was bubbled through the NaCl solutions to remove dissolved CO_2 until the initial pH stabilized. The pH of the solutions was then adjusted to successive initial values between 2.0 and 12.0, by adding either HCl or NaOH and 0.10 g of the prepared thermosensitive composite photocatalyst was added to each of the flasks. The final pH, reached stable after 24 h, was measured and plotted against the initial pH. pH_{pzc} was noted at the pH in which the initial pH equals the final pH. The pH of the solution was measured by using a Mettler-Toledo digital pH meter (model Delta 320-S).

2.5. Thermosensitive studies

The thermoresponsive property of the synthesized composite photocatalysts was evaluated using the swelling ratio (SR, g/g) at different temperatures in double distilled water. The swelling ratio for the composites in swelling equilibrium is termed as equilibrium swelling ratio (ESR, g/g). A sample of a certain weight was transferred between identical baths maintained at either 25 or 45 °C for swelling/deswelling studies. At specific time intervals the sample was withdrawn from the media and blotted with filter paper to remove any excess surface moisture. The swelling ratio was calculated from the following equation:

$$SR = \frac{W_t - W_d}{W_d} \quad (1)$$

where W_t and W_d stand for the sample weights (g) in the swollen state at time t and dried state, respectively.

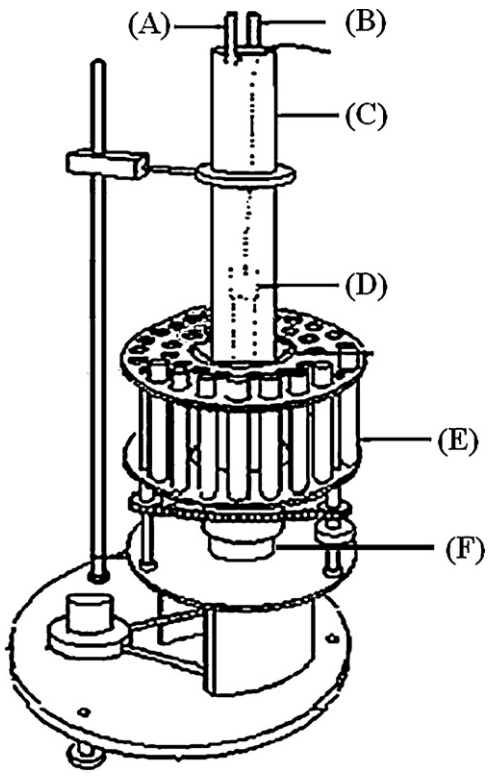

Fig. 1. Schematic diagram of photochemical reactor: (A) cooling inlet, (B) cooling outlet, (C) water-cooled quartz jacket, (D) Xe-arc lamp, (E) quartz reactor, and (F) rotation axis.

2.6. Adsorption and photodegradation of DNBP

The photocatalytic reaction was carried out in a XPA-7 photochemical reactor (Xujiang Electromechanical Plant, Nanjing, China). The photocatalytic reactor consisted of quartz reactors and an illumination source. A 500 W xenon lamp (Institute of Electric Light Source, Beijing) was used as light source to mimic solar irradiation at wavelengths from 300 to 800 nm. The quartz reactors were vertically placed at a fixed distance from the lamp. The distance from the lamp to quartz reactor was about 3.5 cm. The light intensity at the position of quartz tubes was measured using a illumination meter (ST-80C, Beijing Normal University, China) and the average light intensity over the duration of each experiment was calculated to be 2.652×10^4 lx. The reaction system was cooled by circulating water and maintained at certain temperature. The schematic diagram of photochemical reactor is depicted in Fig. 1.

The photocatalytic reaction was carried out in a quartz reactor. The reaction volume was 40 mL with desired concentrations of the thermosensitive composite photocatalyst sample and DNBP. After agitating continuously in the dark for 24 h to ensure establishment of adsorption/desorption and swelling equilibrium, the suspension was irradiated with a 500 W xenon lamp and it was treated as the starting point ($t = 0$) of the photocatalytic reaction, where the concentration of DNBP was designated as C_0. Aliquots of the reaction solution were taken from the suspension at appropriate time

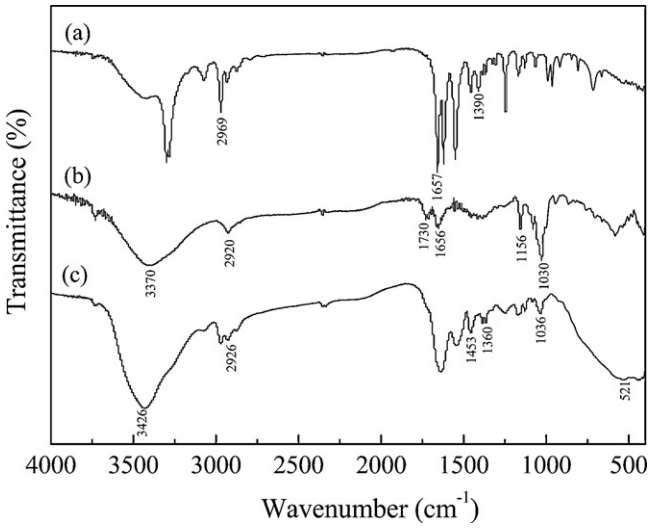

Fig. 2. FTIR spectra of (a) NIPAM, (b) MAH-β-CD, and (c) poly(NIPAM-*co*-MAH-β-CD)/(TiO_2-MWCNTs) composites.

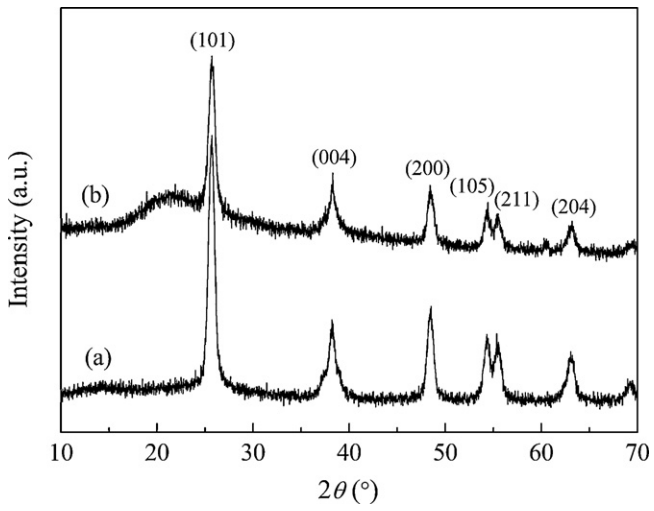

Fig. 3. XRD patterns of (a) pure TiO_2 and (b) poly(NIPAM-*co*-MAH-β-CD)/(TiO_2-MWCNTs) composites.

intervals during the degradation experiments, heated to 45 °C and centrifuged (10,000 × *g*) to completely remove any solid particles. The progress of photocatalytic degradation was monitored with a UV-760CRT UV–Vis spectrophotometer (Shanghai Precision & Scientific Instrument Co. Ltd.) from the absorbance at the wavelength of 376 nm by using a calibration curve [34]. The photocatalytic degradation efficiency (η%) under various conditions was calculated as follows:

$$\eta\% = \frac{C_0 - C_t}{C_0} \times 100 = \frac{A_0 - A_t}{A_0} \times 100 \quad (2)$$

where C_0, A_0 and C_t, A_t represent the concentration and absorbency of DNBP in the photocatalytic reaction solution at the peak of 376 nm before and after irradiation, respectively.

3. Results and discussion

3.1. Characterization results

FTIR spectra of the samples are presented in Fig. 2. For NIPAM, the peaks at 2969, 1657 and 1390 cm^{-1} are due to C—H, O═C—NH_2 and $-CH(CH_3)_2$ of NIPAM, respectively. For MAH-β-CD, a band around 3370 cm^{-1} is attributable to the characteristic stretching vibration of C—OH. The peak at 2920 cm^{-1} corresponds to the —CH_2 asymmetric vibration. The peaks at 1156 and 1030 cm^{-1} are induced by stretching vibrations of C—O and C—O—C of β-CD. The stretching vibration of C═O of MAH could be seen at 1730 cm^{-1}, which confirms the etherification reaction between β-CD and MAH. The FTIR spectrum of the poly(NIPAM-*co*-MAH-β-CD)/(TiO_2-MWCNTs) composite resembled the FTIR spectra of NIPAM and MAH-β-CD. The characteristic bands in NIPAM and MAH-β-CD are also found in the poly(NIPAM-*co*-MAH-β-CD)/(TiO_2-MWCNTs) composite. For the composite, the peaks at 1036 cm^{-1} and 521 cm^{-1} are induced by Ti–O–C vibration and Ti–O stretching vibration, which indicates TiO_2 has reacted with poly(NIPAM-*co*-MAH-β-CD) by–OH.

Fig. 3 shows the XRD patterns of pure TiO_2 and poly(NIPAM-*co*-MAH-β-CD)/(TiO_2-MWCNTs) composites. In the patterns, intensified anatase diffraction peaks of (1 0 1), (0 0 4), (2 0 0), (1 0 5), (2 1 1) (2 0 4) at 25.3°, 37.8°, 48.2°, 54.2°, 55.3° and 62.7° (2θ) are observed. This indicates that only anatase phase can be indexed from the patterns. Moreover, the XRD pattern of the prepared thermosensitive composites contains the same characteristic peaks as that of pure anatase-type TiO_2, but with a lower intensity. This shows that the composites prepared by UV light photoinitiating method do not change the crystalline structure of TiO_2. In the XRD pattern of the poly(NIPAM-*co*-MAH-β-CD)/(TiO_2-MWCNTs) composites, one broad peak can be observed in the region of 2θ = 10–30°. The peak may be assigned to the scattering from the polymer chains in the composites at interplanar spacing and indicates that the polymer had also some degree of crystallinity [35]. The average size of the poly(NIPAM-*co*-MAH-β-CD)/(TiO_2-MWCNTs) composites was estimated to 22.5 nm according to Scherrer's formula.

Fig. 4 shows the variation of the TGA curves of the poly(NIPAM-*co*-MAH-β-CD)/(TiO_2-MWCNTs) composites and the corresponding poly(NIPAM-*co*-MAH-β-CD)/TiO_2-MWCNTs blend. The blend was prepared by merely mixing copolymer of NIPAM and MAH-β-CD with TiO_2-MWCNTs particles and approaching to uniformity thoroughly. The TiO_2 content in poly(NIPAM-*co*-MAH-β-CD)/(TiO_2-MWCNTs) blend was 10%, which is almost the same mass ratio of titania as in poly(NIPAM-*co*-MAH-β-CD)/(TiO_2-MWCNTs) composite. TGA results indicate that poly(NIPAM-*co*-MAH-β-CD)/(TiO_2-MWCNTs) composite undergoes on heating a multistep decomposition process in the temperature 25–850 °C. The weight loss appearing at 25–270 °C is induced by hygroscopic

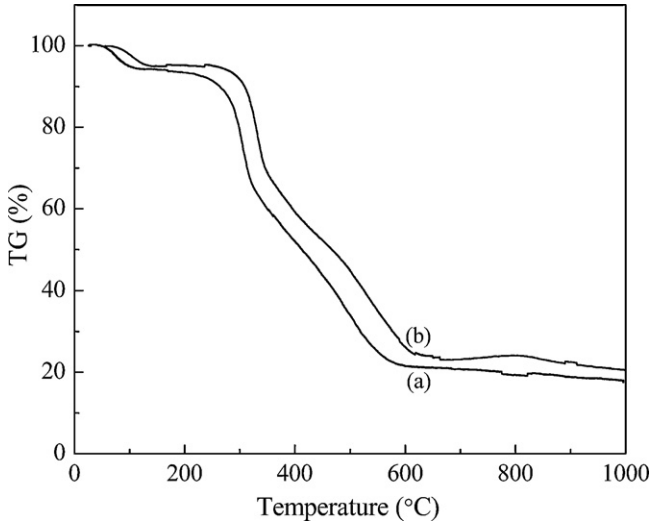

Fig. 4. TGA curves of (a) poly(NIPAM-*co*-MAH-β-CD)/(TiO_2-MWCNTs) blend and (b) poly(NIPAM-*co*-MAH-β-CD)/(TiO_2-MWCNTs) composites.

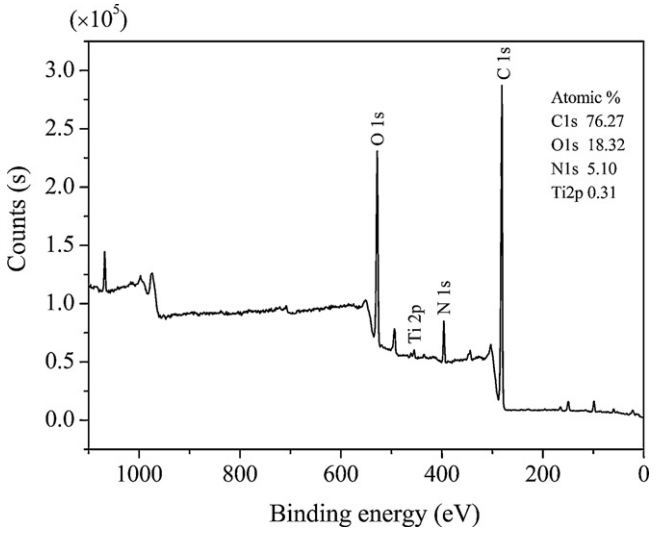

Fig. 5. XPS spectrum of the poly(NIPAM-*co*-MAH-β-CD)/(TiO_2-MWCNTs) composites.

and bound water, whereas those appearing at 270–350 °C are attributed to unreacted monomers and oligomers. Above 350 °C, there is a substantial weight loss in composite due to the combustion of polymers and carbon in the composite. The initial thermal decomposition temperature determined by tangents method and the semi-decomposition temperature of the thermosensitive composite and the corresponding blend are 268/422 °C and 252/406 °C, respectively. TGA results indicate that the poly(NIPAM-*co*-MAH-β-CD)/(TiO_2-MWCNTs) composite exhibits higher thermal stability as compared to poly(NIPAM-*co*-MAH-β-CD)/(TiO_2-MWCNTs) blend. The higher thermal stability of the poly(NIPAM-*co*-MAH-β-CD)/(TiO_2-MWCNTs) could be attributed to some degree of chemical bonding between TiO_2 and polymer chains in the thermosensitive composite.

To investigate the surface structure of the resulting thermosensitive composites, XPS analysis was carried out (Fig. 5). According to the XPS survey spectrum of the sample, the elements of C, O, N, and Ti can be detected and binding energies for C1s, N1s, O1s, and Ti2p are 284.8, 398.9, 531.1, and 458.0 eV, respectively. Fig. 5 shows the very weak signal of Ti2p at 458.0 eV and it can thus be concluded that the poly(NIPAM-*co*-MAH-β-CD)/(TiO_2-MWCNTs) composites are formed from polymer-covered TiO_2-MWCNTs. TiO_2-MWCNTs particles are mainly embedded within the network of a thermally responsive copolymer of NIPAM and MAH-β-CD. This is because only photoelectrons produced in the sheet of 20–30 Å beneath the solid surface can escape and be detected by the photoelectron spectrometer. The elements atomic concentration of C, O, N, and Ti on the sample surface as detected by XPS are 76.27%, 18.32%, 5.10%, and 0.31%, respectively.

Fig. 6 shows the typical TEM images of the TiO_2-MWCNTs nanoparticles and poly(NIPAM-*co*-MAH-β-CD)/(TiO_2-MWCNTs) composites prepared by UV light photoinitiating method. The TEM image of the thermosensitive composites illustrates the similar morphology with that of TiO_2-MWCNTs particles; the particle size is within the range of 20–30 nm, which agrees well with the XRD measurements. The image of the poly(NIPAM-*co*-MAH-β-CD)/(TiO_2-MWCNTs) shows a sample with TiO_2-MWCNTs nanoparticles covered with a layer of copolymer. The TiO_2-MWCNTs nanoparticles are in a dispersed state within the copolymer network. This is because photo-initiated polymerization is fast enough to retain the dispersion stability of nanoparticles [36,37].

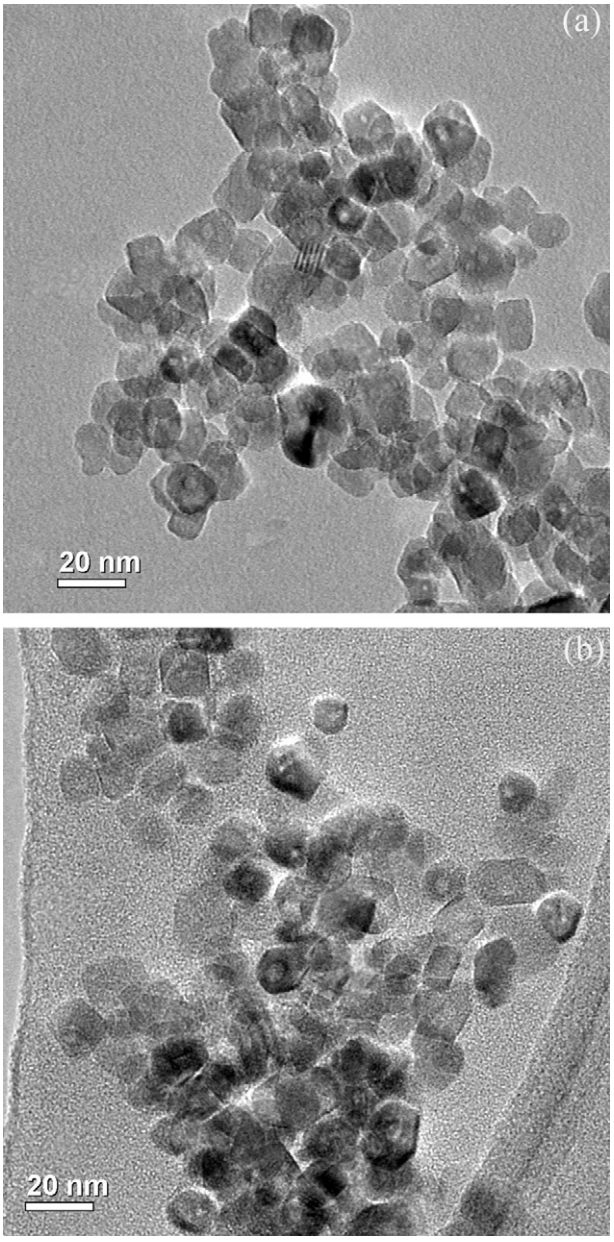

Fig. 6. TEM images of (a) TiO_2-MWCNTs nanoparticles and (b) poly(NIPAM-*co*-MAH-β-CD)/(TiO_2-MWCNTs) composites.

The specific surface area of the samples is measured using the BET method by N_2 adsorption and desorption at 77 K. The prepared thermosensitive composites showed a specific surface area of 163 $m^2\,g^{-1}$. It can be found that the specific surface area of the poly(NIPAM-*co*-MAH-β-CD)/(TiO_2-MWCNTs) composites is almost the same as that of TiO_2-MWCNTs nanoparticles obtained by sol–gel method, indicating the incorporation of TiO_2-MWCNTs nanoparticles into the copolymer network showed no obvious reduction in the specific surface areas of TiO_2-MWCNTs photocatalyst. It is very-well known that the photocatalytic effect of a catalyst is dependent on the surface area. The larger the surface area, the higher will be its photocatalytic activity due to enhanced adsorption of irradiation photons and organic pollutants.

UV–Vis/DRS of the poly(NIPAM-*co*-MAH-β-CD)/(TiO_2-MWCNTs) composites and pure TiO_2 particles are shown in Fig. 7. The absorption maxima of the thermosensitive composites was found to be 406.12 nm, which corresponds to the visible range of the spectrum indicating that the thermosensitive composite

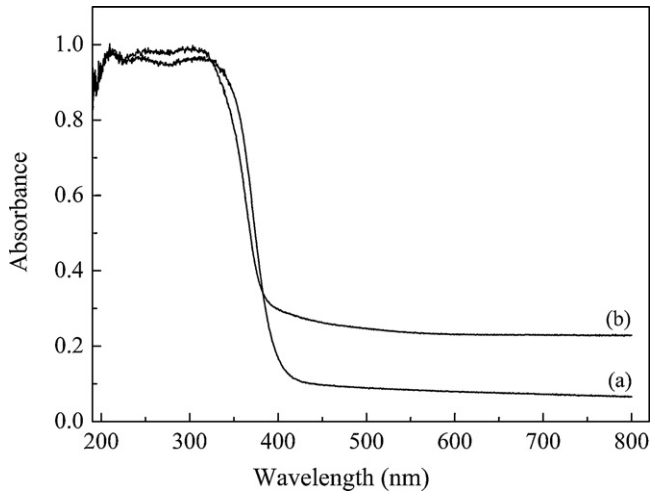

Fig. 7. UV–Vis abosorption spectra of (a) pure TiO_2 and (b) poly(NIPAM-*co*-MAH-β-CD)/(TiO_2-MWCNTs) composites.

catalysts are active in visible light. The prominent red shift of the composite photocatalysts as compared to pure TiO_2 can be attributed to the presence of MWCNTs. The band gap energy was calculated from the absorption maxima by using following equation [38]:

$$E_g\ (\text{eV}) = \frac{1240}{\lambda g} \quad (3)$$

where λg is absorption maxima. The band gap energy of the thermosensitive poly(NIPAM-*co*-MAH-β-CD)/(TiO_2-MWCNTs) was found to be 3.05 eV.

3.2. pH_{pzc} value

The pH_{pzc} value was determined to be approximately 7.48 for the poly(NIPAM-*co*-MAH-β-CD)/(TiO_2-MWCNTs) composites (Fig. 8). At pH lower than the pH_{pzc}, the surface of the thermosensitive composite catalyst is positively charged while at pH greater than pH_{pzc}, the surface of the catalyst becomes negatively charged. For pure TiO_2, the pH_{pzc} value was reported to be 6.5 [39]. The pH_{pzc} value of the composite catalyst is slightly higher than that of pure TiO_2. The shift of pH_{pzc} can be attributed to the deposited copolymer layer with plenty hydroxyl groups.

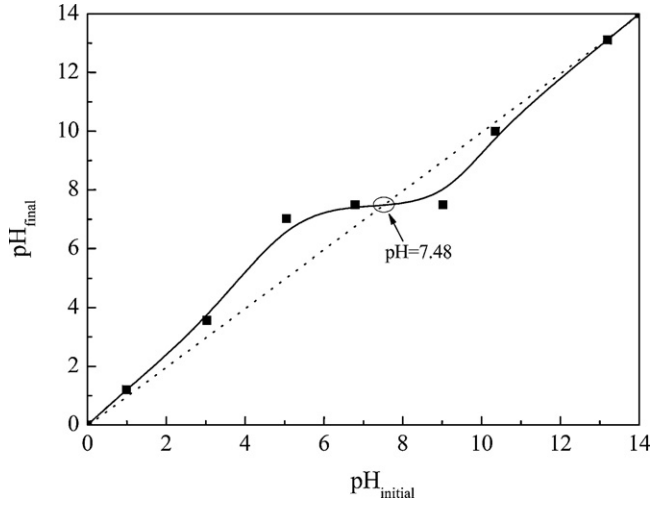

Fig. 8. Plot for the determination of pH_{pzc} of the thermosensitive poly(NIPAM-*co*-MAH-β-CD)/(TiO_2-MWCNTs) composites.

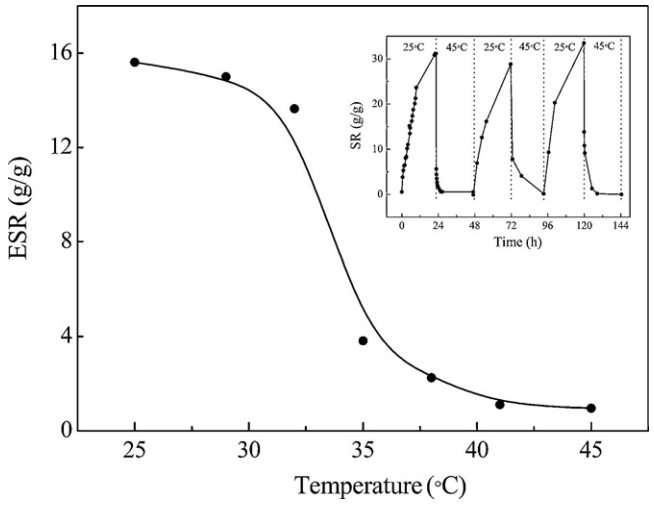

Fig. 9. ESR of the poly(NIPAM-*co*-MAH-β-CD)/(TiO_2-MWCNTs) composites from 25 to 45 °C. Inset shows curves of swelling/deswelling of the thermosensitive composites in response to alternation changes between 25 and 45 °C.

3.3. Thermosensitive analysis

The reversibility of the swelling behavior of the poly(NIPAM-*co*-MAH-β-CD)/(TiO_2-MWCNTs) composites upon temperature cycling above and below its LCST was investigated to analyze the thermoresponsive property of the composites. Fig. 9 shows the swelling/deswelling behavior of the poly(NIPAM-*co*-MAH-β-CD)/(TiO_2-MWCNTs) composites from 25 to 45 °C. It can be seen that the synthesized catalyst was indeed a negative thermoresponsive composite and swelling abruptly decreased at temperature around 34 °C. The temperature at which the thermosensitive composites showed a sharp decrease in swelling was determined to be the LCST, which is approximately the midpoint of the swelling change. When T < LCST, both the hydrogen bonding between H_2O and hydrophilic moiety (O═C—NH) and electrostatic repulsion between ionized carboxylic acid groups of the polymer chains coexist in the composites, which causes the composites to be in the swollen state. On the contrary, when T > LCST, the composites are in the deswollen state, and this indicates that the effect of hydrophobic moiety (—$CH(CH_3)_2$) is dominant in the polymer and H_2O is expelled out of the polymer. As compared with NIPAM, increases in the LCST was observed for the poly(NIPAM-*co*-MAH-β-CD)/(TiO_2-MWCNTs) through the measurement of the temperature dependence of the swelling. This can be attributed the increase in the amount of hydrogen bonds when MAH modified β-CD unit was incorporated into the composites. Fig. 9 inset shows the effect of oscillatory cycling on the thermoresponsive property of the composites at 25 and 45 °C. The thermoresponsive property of the synthesized composites was recoverable after three temperature cycles, which indicated that the composites had thermoreversibility with little loss of thermosensitivity. The controllable thermoresponsive property was retained after the cycle of swelling/deswelling, and this was an indication of the structural stability of the poly(NIPAM-*co*-MAH-β-CD)/(TiO_2-MWCNTs) composites, which is vital for photocatalysis applications of the composites.

3.4. Adsorption and photocatalytic degradation of DNBP

3.4.1. Adsorption isotherms of DNBP on different photocatalysts

The adsorption of organic molecules on photocatalysts plays an important role in the photocatalytic process. Therefore, isothermal adsorption experiments were performed to determine the amount

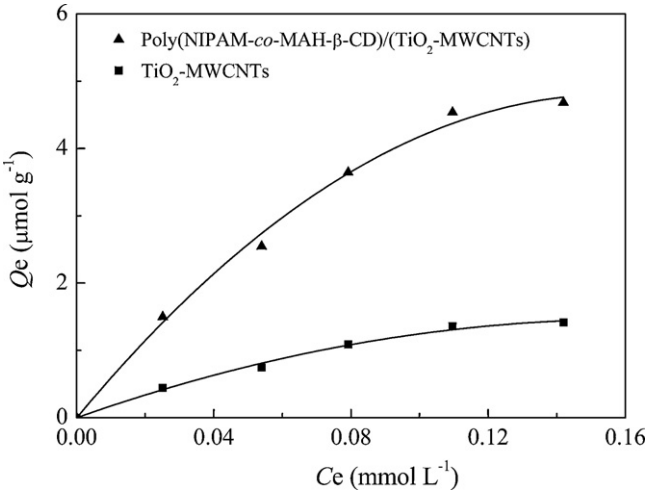

Fig. 10. Adsorption isotherms of DNBP on different photocatalysts.

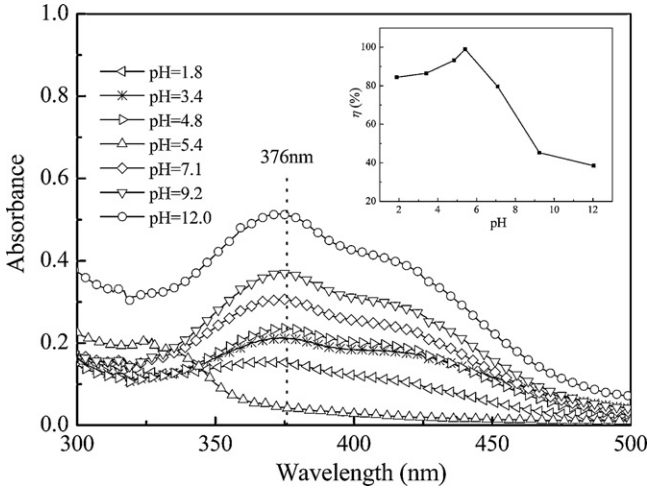

Fig. 11. Absorbance spectra of DNBP degradation in solutions containing poly(NIPAM-*co*-MAH-β-CD)/(TiO_2-MWCNTs) at various pH values. Inset shows effect of pH on the photocatalytic degradation of aqueous solution of DNBP. Conditions: $[DNBP]_0 = 12\ mg\ L^{-1}$, [Catalyst] = 10 g L^{-1}, irradiation time 5 h, $T = 25\ ^\circ C$.

of adsorption of DNBP by contacting the poly(NIPAM-*co*-MAH-β-CD)/(TiO_2-MWCNTs) and TiO_2-MWCNTs photocatalysts with DNBP solutions for 24 h in dark. The temperature was controlled at 25 °C, and the natural pH of the solution of DNBP was situated around 5.4 whatever the initial concentration of DNBP used. The adsorption isotherms of DNBP on different photocatalysts are presented in Fig. 10. Comparing with the adsorption isotherms of DNBP adsorbed on different photocatalysts, those of the TiO_2-MWCNTs and poly(NIPAM-*co*-MAH-β-CD)/(TiO_2-MWCNTs) composites are similar, which perfectly fit Langmuir adsorption isotherm:

$$\frac{1}{Q_e} = \frac{1}{K_L Q_{max} C_e} + \frac{1}{Q_{max}} \quad (4)$$

where Q_e is the amount of DNBP adsorbed per unit mass of the photocatalyst corresponding to surface site density or monolayer adsorption density, C_e the DNBP concentration in solution at the equilibrium, K_L the Langmuir constant, and Q_{max} is the maximum amount of DNBP adsorbed on the photocatalyst. Therefore, the adsorption of DNBP on the poly(NIPAM-*co*-MAH-β-CD)/(TiO_2-MWCNTs) and TiO_2-MWCNTs photocatalysts is a monolayer adsorption. The calculated values of the Langmuir parameters for the adsorption of DNBP on the poly(NIPAM-*co*-MAH-β-CD)/(TiO_2-MWCNTs) and TiO_2-MWCNTs catalysts are respectively $K_L = 7.96 \times 10^{-3}\ L\ \mu mol^{-1}$ and $7.36 \times 10^{-3}\ L\ \mu mol^{-1}$ and $Q_{max} = 9.52\ \mu mol\ g^{-1}$ and $2.91\ \mu mol\ g^{-1}$. It can be observed that the adsorption capacity of the thermosensitive poly(NIPAM-*co*-MAH-β-CD)/(TiO_2-MWCNTs) is higher than that of TiO_2-MWCNTs, which indicates that the incorporation of MAH modified β-CD leads to the enhancement of uptake of DNBP by TiO_2-MWCNTs catalyst. This may be due to the fact that β-CD has a hydrophobic cavity and can adsorb organic pollutants easily.

3.4.2. Effect of pH

The pH of a solution influences adsorption and dissociation of substrate, catalyst surface charge, oxidation potential of the valence band and other physicochemical properties of the system. The effect of pH on the photocatalytic degradation efficiency was studied by keeping all other experimental conditions constant and varying the initial pH of the DNBP solution from 1.8 to 12.0 (Fig. 11). Fig. 11 shows that the peak absorbance of DNBP decreases over 5 h of irradiation as the TiO_2-MWCNTs particles embedded within the thermally responsive copolymer of NIPAM and MAH-β-CD causes photodegradation of DNBP. The degree of degradation increases with pH value up to 6.0, beyond which the photodegradation efficiency starts to decrease. The photocatalytic degradation efficiency stays at a high level (>90%) in the pH range 4.0 to 6.0 and the natural pH of DNBP solution of approximately 5.4 for best performance. It is obvious that photodegradation of DNBP is strongly favored at weak acidic and neutral pH conditions.

The observed effect of the pH on the degradation efficiency is due to different photoreaction mechanisms operable at various pH and pH-dependence of the chemisorptive properties of TiO_2. The possible reaction mechanisms that contribute to DNBP degradation can involve the direct reaction by the photogenerated positive holes or oxidation through successive attacks by hydroxyl radicals or superoxide species [40]. The hydroxyl radical in particular is an extremely strong non-selective oxidant and responsible for the oxidation of organic pollutants.

The pH of the solution affects the formation of hydroxyl radicals as it can be inferred from the following equations [41]:

$$TiO_2 + h\nu \rightarrow TiO_2 + e^-_{cb} + h^+_{vb} \quad (5)$$

$$h^+_{vb} + H_2O \rightarrow HO^\bullet + H^+ \quad (6)$$

$$h^+_{vb} + OH^- \rightarrow HO^\bullet \quad (7)$$

$$HO^\bullet + \text{organic pollutant} \rightarrow \text{degradation products} \quad (8)$$

The very low and high pH values are not available for hydroxyl radicals produced because of the high redox potentials of Eqs. (6) and (7). Besides, the pH of the solution significantly affects the charge on the TiO_2 particles and the positions of the conductance and valence bands [42]. This pH-dependence of surface charge is consistent with the point of zero charge (pzc) of the photocatalyst used. The pH_{pzc} value was determined to be approximately 7.48 for the synthesized poly(NIPAM-*co*-MAH-β-CD)/(TiO_2-MWCNTs) composites, as shown in Fig. 7. DNBP mainly exists in its molecular forms in the acidic medium, with a dissociation of DNBP to anions likely occurring at higher pH values, because the pK_a value of DNBP is 4.26. As a result, alkaline condition is not favorable to the degradation of DNBP due to it possessing similar charges to the synthesized composite photocatalysts, resulting in mutual repulsion hence reduced photocatalytic degradation efficiency.

3.4.3. Effect of catalyst concentration

To understand the optimum catalyst amount required for the effective photocatalytic degradation of DNBP, experiments were performed to study the variations in the photocatalytic degradation efficiency at different catalyst concentration ranging from

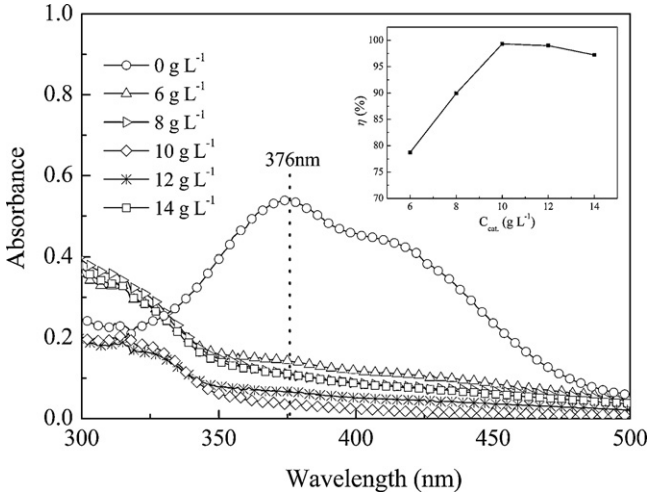

Fig. 12. Absorbance spectra of DNBP degradation in solutions containing different concentrations of poly(NIPAM-*co*-MAH-β-CD)/(TiO_2-MWCNTs). Inset shows effect of the poly(NIPAM-*co*-MAH-β-CD)/(TiO_2-MWCNTs) concentration on the photocatalytic degradation of aqueous solution of DNBP. Conditions: $[DNBP]_0 = 12\ mg\ L^{-1}$, pH 5.41, irradiation time 5 h, $T = 25\ ^\circ C$.

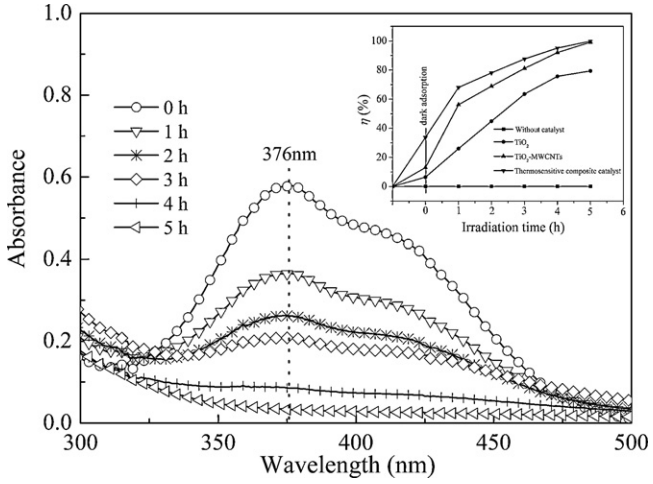

Fig. 13. Absorbance spectra of DNBP degradation in solutions containing poly(NIPAM-*co*-MAH-β-CD)/(TiO_2-MWCNTs) for different irradiation times. Inset shows effect of irradiation time on the photocatalytic degradation efficiency of DNBP for different photocatalysts.

6 to $14\ g\ L^{-1}$. The results of these experiments are shown in Fig. 12. There is a steady decrease in the peak absorbance of DNBP up to $10\ g\ L^{-1}$ of the catalyst beyond which the peak absorbance increases. The degree of photodegradation of DNBP solution increases with increasing amount of photocatalyst, and the highest efficiency was attained at $10\ g\ L^{-1}$. An increase in the photocatalytic degradation efficiency within the range of catalyst concentration from 6 to $10\ g\ L^{-1}$ is due to the increase in number of active sites in the thermosensitive composites available for the reaction, which in turn increases the rate of radical formation. The surplus addition of the catalysts makes the solution more viscous and turbid which in turn reduces the probability of degradation reaction between DNBP and •OH radicals and the light penetration reaching the composite surface, resulting in reduced photocatalytic degradation efficiency. The result indicates that an optimized catalyst concentration ($10\ g\ L^{-1}$) is necessary for enhancing the degradation efficiency.

3.4.4. Effect of irradiation time

The effect of irradiation time on the photocatalytic degradation of DNBP from its aqueous solution was investigated under the optimized experimental conditions. The results are illustrated in Fig. 13. As can clearly be seen, the characteristic absorption peak of DNBP at 376 nm disappeared progressively upon visible light irradiation indicating the degradation of DNBP was taking place. The solution without catalysts has almost no degradation after irradiation, suggesting that the degradation of DNBP predominately occurred via photocatalysis rather than photolysis. Then, pure TiO_2, TiO_2-MWCNTs and poly(NIPAM-*co*-MAH-β-CD)/(TiO_2-MWCNTs) composite photocatalysts were added and the degree of degradation under visible light irradiation for the same illumination time was examined. After 5 h irradiation, the degree of photocatalytic degradation of DNBP by pure TiO_2 was 86%. However, the TiO_2-MWCNTs nanoparticles and poly(NIPAM-*co*-MAH-β-CD)/(TiO_2-MWCNTs) composites can achieve almost 100% DNBP removal at the same irradiation time. The results indicate that TiO_2-MWCNTs can degrade DNBP more effectively than pure TiO_2. There was nothing in the formation of poly(NIPAM-*co*-MAH-β-CD)/(TiO_2-MWCNTs) composites to affect the degradation efficiency of TiO_2-MWCNTs photocatalyst, for the thermosensitive poly(NIPAM-*co*-MAH-β-CD)/(TiO_2-MWCNTs) composites can evenly disperse in water and form transparent solution. For pure TiO_2, TiO_2-MWCNTs and poly(NIPAM-*co*-MAH-β-CD)/(TiO_2-MWCNTs) composites, the photocatalytic degradation efficiency increases with time, up to 5 h, and, thereafter, it levels off. This indicates that photocatalytic degradation of DNBP with catalysts for 5 h is the optimum irradiation time.

3.4.5. Effect of concentration of DNBP and kinetics of photocatalytic degradation

The effect of initial concentrations of DNBP on the photocatalytic degradation efficiency was investigated by varying the initial concentration from 5 to 25 $mg\ L^{-1}$. The results show that the photocatalytic degradation efficiency of DNBP decreases with an increase in the initial concentration of DNBP. This can be as a result of blocking of the photocatalytically active sites on the catalyst and reducing the interaction of photons with these sites. Besides, a fraction of light may be absorbed by the DNBP molecules in aqueous solution rather than the catalyst particles for high DNBP concentration, which can also reduce the efficiency of the photocatalytic reaction to a certain extent. Photocatalytic reactions on TiO_2 surface can be expressed by a modified Langmuir–Hinshelwood model:

$$r = -\frac{dC}{dt} = \frac{k_r K C}{1 + KC} \tag{9}$$

The intergral form of Eq. (9) is:

$$t = \left(\frac{1}{k_r K}\right) \ln\left(\frac{C_0}{C}\right) + \frac{C_0 - C}{k_r} \tag{10}$$

where t refers to the irradiation time, C_0 is initial concentration of DNBP and C is the concentration of DNBP at time t, r represents the rate of degradation, K is the equilibrium constant for the adsorption of DNBP on the catalyst and k_r reflects the limiting rate of the reaction at the maximum coverage at the experimental conditions.

At low initial concentration of DNBP, the second term in Eq. (10) becomes insignificant and hence it can be neglected:

$$\ln\left(\frac{C_0}{C}\right) = k_r K t = k_{app} t \tag{11}$$

where k_{app} is the apparent rate constant of the photocatalytic degradation reaction.

The applicability of Langmuir–Hinshelwood equation for the photocatalytic degradation of DNBP has been confirmed by the good linearity between $\ln(C_0/C)$ versus t plot for each DNBP concentration values studied (Fig. 14). The apparent rate constant, k_{app} (min^{-1}) calculated from the slopes of the lines decreases with an

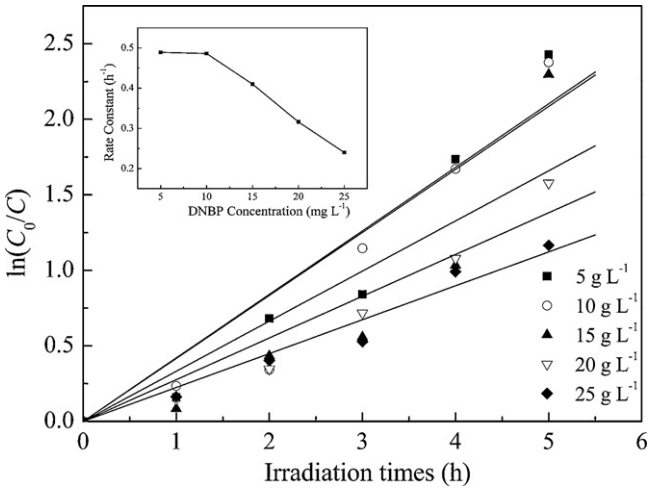

Fig. 14. Kinetics of DNBP degradation for various initial concentrations in the presence of poly(NIPAM-*co*-MAH-β-CD)/(TiO_2-MWCNTs) composites. Inset shows rate constants for the photocatalytic degradation of DNBP for various initial concentrations using the poly(NIPAM-*co*-MAH-β-CD)/(TiO_2-MWCNTs) composite photocatalyst.

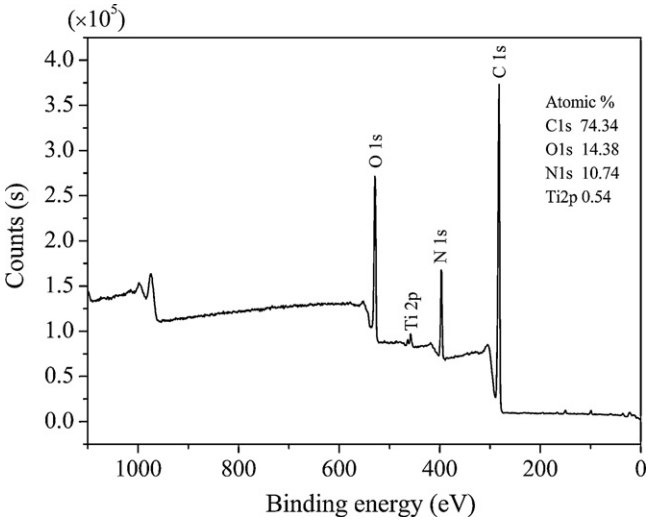

Fig. 16. XPS spectrum of the poly(NIPAM-*co*-MAH-β-CD)/(TiO_2-MWCNTs) composites after 5 h solar simulated irradiation during the photodegradation of DNBP.

increase in the initial concentration of DNBP. The control experiment, where DNBP in solution was irradiated in the absence of the thermosensitive composites under similar conditions yielded a null rate constant and confirmed that DNBP degradation was achieved via photocatalysis alone.

3.4.6. *The reproducibility and stability of the catalyst*

The repetitive use of is very important for the practical application of photocatalyst. So, the repetitive use of the thermosensitive composite photocatalysts was also studied (Fig. 15). After the completion of the degradation, the catalyst at the end of I cycle was collected, rinsed with water and utilized for the next cycle by keeping other reaction conditions constant. Noticeably, the catalysis efficiency of the thermosensitive composites was still higher than 90% after be used for six cycles. This indicates that the photocatalytic activity of the synthesized composites has good repeatability. From the experimental results, we can infer that TiO_2-MWCNTs particles in the poly(NIPAM-*co*-MAH-β-CD)/(TiO_2-MWCNTs) composites are not released into the aqueous solution. Otherwise, the photocatalysis efficiency would decrease sharply because the copolymer of NIPAM and MAH-β-CD has no photocatalytic activity.

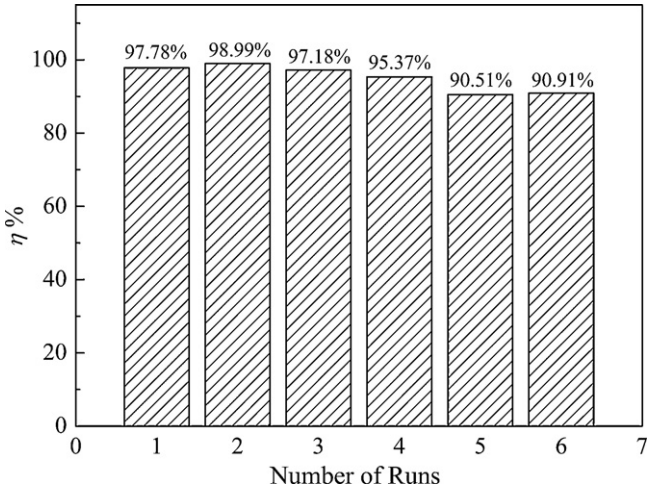

Fig. 15. Results of recycling studies. Conditions: $[DNBP]_0 = 12\,mg\,L^{-1}$, [Catalyst] = 10 g L^{-1}, pH 5.41, irradiation time 5 h, $T = 25\,^{\circ}C$.

The reduction in the photocatalytic degradation efficiency among the cycles may be due to the formation of by-products and their accumulation in the cavities and on the active surface sites of the catalyst. The results reported in this study demonstrate that the visible light can be used for photocatalytic degradation of chemical contaminants with the thermosensitive composites without rapid decomposition of the polymeric matrix. Thus, the thermosensitive composites are excellent candidates for remediation processes that can re-use and re-cycle the titania photocatalyst easily.

The stability is also a crucial problem for the thermosensitive composite photocatalysts. In order to evaluate the stability of the synthesized poly(NIPAM-*co*-MAH-β-CD)/(TiO_2-MWCNTs) composites, a simple weight measurement of the composites in the dried state was performed before and after photocatalytic degradation reaction. It was found that weight loss was about 0.32% for the poly(NIPAM-*co*-MAH-β-CD)/(TiO_2-MWCNTs) after simulated solar irradiation of 5 h, indicating that the synthesized composites had high stability and favorable degradability resistance of organic support. The high stability of the thermosensitive composite catalysts can also be confirmed by the XPS spectra. Fig. 16 presents XPS of the surface of the poly(NIPAM-*co*-MAH-β-CD)/(TiO_2-MWCNTs) composites after 5 h irradiation during the photodegradation of DNBP. It can be found that during DNBP degradation, the Ti element atomic concentration changes slightly on the composite catalyst surface after irradiation of 5 h. Meanwhile, the signal of Ti2p around 458.0 eV increases slightly on the catalyst surface after photocatalytic degradation reaction. This indicates that after 5 h reaction, most TiO_2-MWCNTs particles are still embedded within the copolymer network and that the polymer chains surrounding the TiO_2-MWCNTs particles are seldom cracked and detaches from the TiO_2-MWCNTs particles.

3.5. *Postulated mechanism*

Based on the experimental results above, it could be concluded that the poly(NIPAM-*co*-MAH-β-CD)/(TiO_2-MWCNTs) composites exhibit better photocatalytic activity than pure TiO_2 in the degradation of DNBP under visible light irradiation. This can be attributed to the electron transfer between MWCNTs and TiO_2, which can enhance the photocatalytic activity of the composites photocatalysts effectively [16]. The incorporation of MAH modified β-CD unit into the thermosensitive composites provides an apparently additive effect on their adsorption capacities. The thermosensitive

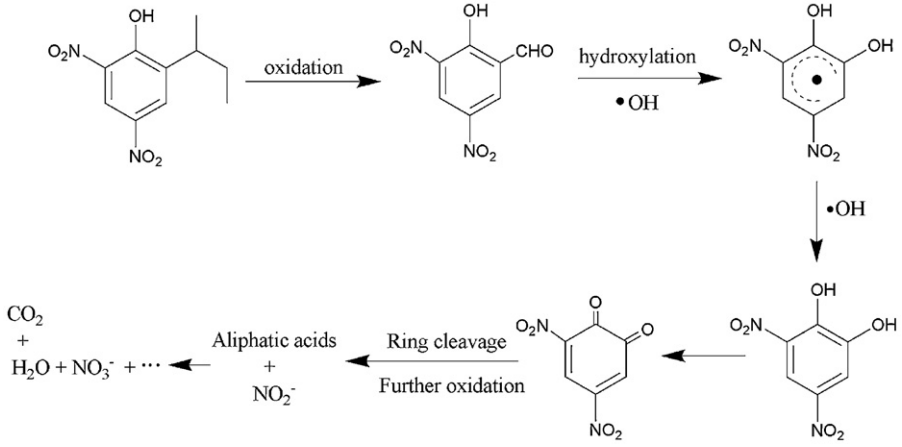

Scheme 1. Postulated photocatalytic degradation pathway of DNBP.

composites dissolve in water to form transparent solution at room temperature, which in turn increases the dispersion stability of the photocatalysts and the light penetration reaching the photocatalyst surface, resulting in increased photocatalytic degradation efficiency.

GC/MS analyses were used to detect the intermediate products of DNBP degradation. The samples taken at different time intervals during the photocatalytic degradation reaction were filtered and evaporated on a rotatory evaporator to concentrate to 5 mL at 40 °C. The anhydrous extracts were dissolved in 25 mL of diethyl ether and sonicated for 10 min. After diethyl ether was removed from the mixture under reduced pressure, 2 mL of methanol and 1 mL of trimethylsulfonium hydroxide were added. After the addition was complete the reaction mixture was agitated continuously for 12 min at 50 °C and the resulting samples were injected into the GC/MS system (Agilent 6890 GC and 5793 MS) for analysis. The flow rate of carrier gas was 0.5 mL min^{-1} and the oven temperature was programmed as follows: isothermal at 40 °C for 5 min, from 40 to 280 °C at 5 °C min^{-1}, and isothermal at 280 °C for 1 min. From the GC/MS analyses described above, the main intermediate compounds during photocatalytic degradation of DNBP were identified as 3,5-dinitro-salicylaldehyde, 3,5-dinitrocatechol, and 4-nitrocatechol. Their molecular weights were 212, 200, and 155, respectively. These intermediates compounds may be subjected to further degradation, eventually leading to aromatic ring opening and the formation of a series of aliphatic mono- and dicarboxylic acids which could be mineralized eventually to CO_2 and H_2O. Scheme 1 shows the proposed stepwise photocatalytic degradation of DNBP in 5 h with the thermosensitive composite photocatalyst/simulated solar light, which was based on the analysis result by the GC–Mass spectrometer. In the TiO_2 photocatalytic degradation process, oxidative degradation of DNBP occurred generally by the attack of •OH radicals, known as highly reactive electrophilic oxidants. The attack of electrophilic •OH radical occurred at ring position activated by the presence of the corresponding substituents in DNBP. Thus, the initial DNBP destruction was likely occurred with *sec*-butyl oxidation. The reaction proceeded with subsequent attacks of hydroxyl radicals in *ortho* and *para* positions with respect to phenolic hydroxyl group, resulting in hydroxylated dinitrophenol through the formation of dihydroxynitrocyclohexadienyl radicals. On subsequent •OH radical attack, the primary hydroxylated dinitrophenol formed species with higher oxygen to carbon content. In turn, they may be subjected to further attack by •OH radical, eventually leading to aromatic ring opening and the formation of a series of small molecules like oxalic and acetic acids et al. Finally, the reaction intermediates were mineralized into CO_2, H_2O and NO_3^- ion during DNBP degradation.

4. Conclusions

The novel thermosensitive poly(NIPAM-*co*-MAH-β-CD)/(TiO_2-MWCNTs) composite photocatalysts with high activity for DNBP degradation were easily synthesized using MAH modified β-CD to copolymerize with NIPAM by UV light photoinitiating method. The characterizations results indicate that the synthesized composite photocatalysts are mainly in spherical shapes with particle size in the range of 20–30 nm. The TiO_2-MWCNTs particles were dispersed well within the copolymer of NIPAM and MAH-β-CD. The synthesized composites can be activated by absorbing both the ultraviolet and visible light, which are of benefit to efficient photocatalytic reactions under natural light. The poly(NIPAM-*co*-MAH-β-CD)/(TiO_2-MWCNTs) composites showed a negative thermoresponsive volume phase transition and the swelling of the composites exhibited a high sensitivity to external temperature stimuli. The synthesized composite has a favorable adsorption of DNBP, and higher photocatalytic efficiency for degradation of DNBP under visible light irradiation. The satisfactory photocatalytic degradation efficiency can be achieved with the use of optimal operational parameters. The optimal conditions were a DNBP concentration of 12 mg L^{-1} at pH 5.41 with catalyst concentration of 10 g L^{-1} under visible light irradiation for 5 h at room temperature. Further kinetic studies revealed that the photocatalytic degradation followed pseudo-first-order kinetics with respect to DNBP concentration. The novel composite photocatalysts prepared in this study have repeatability. The results of the study showed the feasible and potential use of the novel thermosensitive composites in photocatalyitc degradation of targeted contaminants by controlling temperature.

Acknowledgements

We gratefully acknowledge the financial support provided by the National Natural Science Foundation of China (Grant No. 20977013). Partial support by the Fundamental Research Funds for the Central Universities (DUT10LK26) is also acknowledged.

References

[1] J. Nakajima, S. Tazikani, H. Tomioka, Journal of the Japan Petroleum Institute 46 (2003) 359–367.
[2] M.J.M. Wells, L.Z. Yu, Journal of Chromatography A 885 (2000) 237–250.
[3] U.S. Environmental Protection Agency, Lab Cert Bulletin, EPA-815-N-00-001a, January 2000.
[4] M. Pera-Titus, V. Garcia-Molina, M. Banos, J. Gimenez, S. Esplugas, Applied Catalysis B: Environmental 47 (2004) 219–256.
[5] S. Esplugas, J. Giménez, S. Contreras, E. Pascual, M. Rodrıïguez, Water Research 36 (2002) 1034–1042.

[6] A. Fujishima, X. Zhang, D.A. Tryk, Surface Science Reports 63 (2008) 515–582.
[7] A.D. Paola, E. García-López, G. Marcì, L. Palmisano, Journal of Hazardous Materials 211–212 (2012) 3–29.
[8] C. Xu, R. Killmeyer, M.L. Gray, S.U.M. Khan, Applied Catalysis B: Environmental 64 (2006) 312–317.
[9] G. Wu, T. Nishikawa, B. Ohtani, A. Chen, Chemistry of Materials 19 (2007) 4530–4537.
[10] Y. Cong, J. Zhang, F. Chen, M. Anpo, Journal of Physical Chemistry C 111 (2007) 6976–6982.
[11] T. Tachikawa, Y. Takai, S. Tojo, M. Fujitsuka, H. Irie, K. Hashimoto, T. Majima, Journal of Physical Chemistry B 110 (2006) 13158–13165.
[12] S. Liu, X. Chen, Journal of Hazardous Materials 152 (2008) 48–55.
[13] X. Yang, C. Cao, L. Erickson, K. Hohn, R. Maghirang, K. Klabunde, Journal of Catalysis 260 (2008) 128–133.
[14] H. Sun, Y. Bai, Y. Cheng, W. Jin, N. Xu, Industrial and Engineering Chemistry Research 45 (2006) 4971–4976.
[15] H. Wang, H.L. Wang, W.F. Jiang, Z.Q. Li, Water Research 43 (2009) 204–210.
[16] H. Wang, H.L. Wang, W.F. Jiang, Chemosphere 75 (2009) 1105–1111.
[17] S.X. Li, F.Y. Zheng, X.L. Liu, F. Wu, N.S. Deng, J.H. Yang, Chemosphere 61 (2005) 589–594.
[18] A.P. Xagas, M.C. Bernard, A.H.L. Goff, N. Spyrellis, Z. Loizos, P. Falaras, Journal of Photochemistry and Photobiology A: Chemistry 132 (2000) 115–120.
[19] A. Molinari, R. Amadelli, L. Antolini, A. Maldotti, P. Battioni, D. Mansuy, Journal of Molecular Catalysis A: Chemical 158 (2000) 521–531.
[20] F. Yuen, K.C. Tam, Soft Matter 6 (2010) 4613–4630.
[21] T. Rajh, L.X. Chen, K. Lukas, T. Liu, M.C. Thurnauer, D.M. Tiede, Journal of Physical Chemistry B 106 (2002) 10543–10552.
[22] J. Gao, B.J. Frisken, Langmuir 19 (2003) 5212–5216.
[23] M.S. Kang, V.K. Gupta, Journal of Physical Chemistry B 106 (2002) 4127–4132.
[24] C.A. Coutinho, V.K. Gupta, Journal of Colloid and Interface Science 315 (2007) 116–122.
[25] N. Shamim, L. Hong, K. Hidajat, M.S. Uddin, Separation and Purification Technology 53 (2007) 164–170.
[26] Y.H. Lien, T.M. Wu, J.H. Wu, J.W. Liao, Journal of Nanoparticle Research 13 (2011) 5065–5075.
[27] R. Narain, M. Gonzales, A.S. Hoffman, P.S. Stayton, K.M. Krishnan, Langmuir 23 (2007) 6299–6304.
[28] K. Komori, H. Matsui, T. Tatsuma, Bioelectrochemistry 65 (2005) 129–134.
[29] Y. Wang, J. Zhang, W. Zhang, M. Zhang, Journal of Organic Chemistry 74 (2009) 1923–1931.
[30] S.Q. Wang, Q.L. Liu, A.M. Zhu, European Polymer Journal 47 (2011) 1168–1175.
[31] C.A. Coutinho, V.K. Gupta, Journal of Colloid and Interface Science 333 (2009) 457–464.
[32] R.H. Pelton, P. Chibante, Colloids and Surfaces 20 (1986) 247–256.
[33] M.V. Lopez-Ramon, F. Stoeckli, C. Moreno-Castilla, F. Carrasco-Marin, Carbon 37 (1999) 1215–1221.
[34] H.L. Wang, W.F. Jiang, Industrial and Engineering Chemistry Research 46 (2007) 5405–5411.
[35] W. Feng, E. Sun, A. Fujii, H. Wu, K. Nihara, K. Yoshino, Bulletin of the Chemical Society of Japan 73 (2000) 2627–2633.
[36] M.R. Karim, K.T. Lim, M.S. Lee, K. Kim, J.H. Yeum, Synthetic Metals 159 (2009) 209–213.
[37] H.L. Wang, D.Y. Zhao, W.F. Jiang, Synthetic Metals 162 (2012) 296–302.
[38] A. Mills, R.H. Davies, D. Worsley, Chemical Society Reviews 22 (1993) 417–425.
[39] A.G. Rincón, C. Pulgarin, Applied Catalysis B: Environmental 51 (2004) 281–300.
[40] D. Yang, X. Ni, W. Chen, Z. Weng, Journal of Photochemistry and Photobiology A: Chemistry 195 (2008) 323–329.
[41] K.M. Parida, N. Sahu, N.R. Biswal, B. Naik, A.C. Pradhan, Journal of Colloid and Interface Science 318 (2008) 231–237.
[42] M.R. Sohrabi, M. Ghavami, Journal of Hazardous Materials 153 (2008) 1235–1239.